IAI
Journals.ASM.org

Plasmodium yoelii Macrophage Migration Inhibitory Factor Is Necessary for Efficient Liver-Stage Development

Jessica L. Miller,[a] Anke Harupa,[a] Stefan H. I. Kappe,[a,b] and Sebastian A. Mikolajczak[a]

Seattle Biomedical Research Institute, Seattle, Washington, USA,[a] and Department of Global Health, University of Washington, Seattle, Washington, USA[b]

Mammalian macrophage migration inhibitory factor (MIF) is a multifaceted cytokine involved in both extracellular and intracellular functions. Malaria parasites express a MIF homologue that might modulate host immune responses against blood-stage parasites, but the potential importance of MIF against other life cycle stages remains unstudied. In this study, we characterized the MIF homologue of *Plasmodium yoelii* throughout the life cycle, with emphasis on preerythrocytic stages. *P. yoelii* MIF (Py-MIF) was expressed in blood-stage parasites and detected at low levels in mosquito salivary gland sporozoites. MIF expression was strong throughout liver-stage development and localized to the cytoplasm of the parasite, with no evidence of release into the host hepatocyte. To examine the importance of Py-MIF for liver-stage development, we generated a Py-*mif* knockout parasite (*P. yoelii* Δ*mif*). *P. yoelii* Δ*mif* parasites grew normally as asexual erythrocytic-stage parasites and showed normal infection of mosquitoes. In contrast, the *P. yoelii* Δ*mif* strain was attenuated during the liver stage. Mice infected with *P. yoelii* Δ*mif* sporozoites either did not develop blood-stage parasitemia or exhibited a delay in the onset of blood-stage patency. Furthermore, *P. yoelii* Δ*mif* parasites exhibited growth retardation *in vivo*. Combined, the data indicate that *Plasmodium* MIF is important for liver-stage development of *P. yoelii*, during which it is likely to play an intrinsic role in parasite development rather than modulating host immune responses to infection.

Macrophage migration inhibitory factor (MIF) is a pleiotrophic factor involved in both innate and adaptive immune responses (reviewed in references 10 and 34). MIF is conserved throughout higher eukaryotes, and homologues have been identified in several disease-causing parasites, including *Leishmania* (21), several pathogenic worms (47), and *Plasmodium* (2, 40). *Plasmodium* species are the etiologic agents of malaria and are responsible for the illness of 300 to 500 million people and the death of 800,000 people annually (49). These parasites are transmitted to a mammalian host during a bite from an *Anopheles* mosquito, which deposits *Plasmodium* sporozoites into the skin. The sporozoites migrate to the liver, where they infect hepatocytes. One replicating parasite within a hepatocyte can generate tens of thousands of erythrocyte-infectious forms to initiate blood-stage infection (reviewed in reference 31). Several *Plasmodium* species, including the human malaria-causing species *Plasmodium falciparum* and *P. vivax* and the rodent malarial species *P. berghei* and *P. yoelii*, contain *MIF* homologues (PlasmoDB entries PFL1420w, PVX_124095, PBANKA_144400, and PY05452).

MIF is most commonly thought of as a proinflammatory cytokine and chemokine (38) that can induce the secretion of tumor necrosis factor (TNF), interleukin 18 (IL-18), nitric oxide, IL-6, and other proinflammatory factors (9, 22, 28). It is expressed by multiple cell types, including lymphocytes (4), macrophages (9), and epithelial cells (18). MIF lacks a canonical secretion signal and is released from immune cells in an unknown manner in response to cytokines (e.g., TNF or gamma interferon) (9) and microbial products (5). Hence, it is commonly associated with inflammatory responses during infections such as sepsis (7) and malaria (3, 19, 29). It has been shown that MIF binds to a CD74 and CD44 receptor complex and induces sustained extracellular signal-regulated kinase 1/2 (ERK1/2) mitogen-activated protein kinase (MAPK) activation. This interaction eventually leads to NF-κB activation and the transcription of proinflammatory molecules (27, 37, 41). MIF can also bind to a heterodimer of CD74 and CXCR2/4 to act as a chemokine inducing recruitment of macrophages (6, 38). In addition to its cytokine functions, MIF has multiple intracellular roles. For example, MIF can inhibit the immune regulatory transcription factor AP-1 (23) and downregulates p53 and p53-associated signaling pathways (17, 37). Furthermore, MIF is able to regulate cell division and is necessary for normal progression of the cell cycle (33). MIF further distinguishes itself from other cytokines by concurrently possessing enzymatic capabilities. It contains both an oxidoreductase active site and a tautomerase active site (24, 36), but no substrates for either site have been identified *in vivo* (14).

Although the protein identity between mammalian and *Plasmodium* MIF proteins is low (29% for *P. falciparum*), the structure is well conserved, including the presence of tautomerase and oxidoreductase sites (2, 13). It has been shown that *Plasmodium* MIF is highly expressed in erythrocyte-stage trophozoites and schizonts, and it is thought that it is released into the host bloodstream during schizont rupture (2, 45). Accordingly, antibodies against parasite MIF have been isolated from sera of both previously and currently infected hosts (11, 45). *P. falciparum* MIF (Pf-MIF) has also been detected in the blood of infected patients (2, 16, 39). In addition, it was shown that *Plasmodium* MIF conserves the chemotactic but not cytokine functions of mammalian MIF (2, 45). Interestingly, *P. berghei* MIF coimmunoprecipitates with human

Received 29 August 2011 **Returned for modification** 29 September 2011
Accepted 6 January 2012
Published ahead of print 17 January 2012
Editor: J. H. Adams
Address correspondence to Sebastian A. Mikolajczak, sebastian.mikolajczak@seattlebiomed.org.
Supplemental material for this article may be found at http://iai.asm.org/.

doi:10.1128/IAI.05861-11

CD74 (13) and can induce MAPK signaling (40). This suggests that *Plasmodium* MIF can interact with and signal through host MIF receptors *in vitro*. The *in vivo* role for *Plasmodium* MIF during blood stages, however, is still unclear. Interestingly, two groups have shown that artificially increased levels of *Plasmodium* MIF, induced by either infection with a MIF-overexpressing parasite or injection of recombinant protein, result in a reduction in parasite virulence. This suggests that *Plasmodium* MIF may be involved in dampening acute infection and allowing prolonged infection (40, 45).

While several groups have examined *Plasmodium* MIF during blood-stage malaria (2, 11, 40, 45), the importance of MIF during development of preerythrocytic stages has not yet been evaluated. Using the *P. yoelii* rodent malaria model, we showed that *P. yoelii* MIF (Py-MIF) is expressed predominantly during blood-stage development and liver-stage development, during which it is confined to the parasite cytoplasm. Furthermore, by utilizing a MIF-deficient *P. yoelii* knockout parasite, we determined that *Plasmodium* MIF is required for efficient progression through the liver stage of infection.

MATERIALS AND METHODS

Experimental animals, parasites, and cell lines. Six- to eight-week-old female BALB/cJ (for *in vivo* infection studies) or Swiss Webster (SW) (for parasite cycle maintenance) mice were purchased from the Jackson Laboratory (Bar Harbor, ME) or Harlan (Indianapolis, IN). Animal handling was conducted according to Institutional Animal Care and Use Committee-approved protocols. Wild-type (WT) *P. yoelii* 17XNL (nonlethal strain) clone 1.1 (48) and *P. yoelii* Δ*mif* parasites were cycled between SW mice and *Anopheles stephensi* mosquitoes. Infected mosquitoes were maintained on sugar water at 24°C and 70% humidity. Salivary gland sporozoites were extracted from infected mosquitoes on day 14 post-blood meal infection as described before (26, 43). The human hepatoma cell line HepG2-CD81 (42) was used for all *in vitro* assays and was maintained in Dulbecco's modified Eagle's medium (DMEM) (Gibco) supplemented with antibiotics (penicillin and streptomycin) and 10% fetal calf serum (FCS).

Generation of *P. yoelii* Δ*mif* parasites. Targeted deletion of Py-*mif* by double-crossover homologous recombination was achieved by constructing a replacement plasmid in a modified version of the b3D.DT^H.^D targeting vector containing a red fluorescent protein (RFP) cassette (30). Design of this construct was based on the *P. berghei mif* (Pb-*mif*) annotation, which was described previously (2) and confirmed in *P. yoelii* (45). *P. yoelii* 17XNL genomic DNA (gDNA) was used as a template to amplify a 0.5-kb fragment of the 5′-untranslated region (5′UTR) and a 0.7-kb fragment of the 3′UTR of Py-*mif*, using oligonucleotide primers PyMIF-1 SacII forward (F), PyMIF-2 ApaI reverse (R), PyMIF-3 ApaI F, and PyMIF-4 NotI R (primer sequences are provided in Table S1 in the supplemental material). PyMIF-2 F and PyMIF-3 R contained a unique ApaI site and overlapping sequences. The 5′UTR and 3′UTR fragments were then combined by sequence overlap extension PCR, and the resulting fragment was inserted into the transfection plasmid between SacII and NotI restriction enzyme sites. The resulting plasmids were digested with ApaI between the 5′UTR and the 3′UTR to linearize the plasmid for transfection. Transfection of *P. yoelii* 17XNL parasites by use of an Amaxa Nucleofector device (Lonza Cologne GmbH, Germany), resistant parasite selection, and recombinant parasite cloning by serial limiting dilution were all conducted as described elsewhere (20). We obtained two independent *P. yoelii* Δ*mif* clonal parasite populations (*P. yoelii* Δmif_1 and *P. yoelii* Δmif_2), from two independent transfections. To confirm the targeted deletion and genetic recombination, integration-specific gDNA PCR amplification of the *P. yoelii* Δ*mif* locus was generated using the specific primer combinations 5′ test (TgF and PyMIFTestF) and 3′ test (PyMIFTestR and TgR). The MIF open reading frame (ORF) was amplified using the primers Sp/PyMIF and Asp/PyMIF (primer sequences are provided in Table S1).

RT-PCR. Total RNA was extracted using TRIzol reagent (Invitrogen) from *P. yoelii* salivary gland sporozoites (2×10^6), mixed blood-stage parasites (1×10^7 infected red blood cells were isolated from an infected mouse by heart puncture bleeding and serial limiting dilution of infected blood), or infected livers and then treated with Turbo DNase (Ambion). cDNA synthesis was performed using a SuperScript III Platinum two-step quantitative reverse transcription-PCR (qRT-PCR) kit according to the manufacturer's instructions (Invitrogen). The sequences of specific primers used for amplification from cDNA are listed in Table S2 in the supplemental material. Thirty-five PCR amplification cycles were performed (95°C for 30 s for DNA denaturation and 60°C for 4 min for primer annealing and DNA strand extension). For semiquantitative PCR (QPCR), a standard curve was generated using 1:4 serial dilutions of a reference cDNA sample for PCR amplification of all target PCR products. Experimental samples were compared to this standard curve to give relative transcript abundances. For determination of parasite biomass (see Fig. 4), the average transcript abundance for WT-infected livers was normalized to 1.

IFAs. (i) Salivary gland sporozoites. Salivary gland sporozoites were isolated and fixed with formalin (Sigma, St. Louis, MO) for 10 min at room temperature. Fixed sporozoites were applied to a polylysine-treated slide, which was housed in a wet chamber at 4°C overnight. Sporozoites were washed twice with phosphate-buffered saline (PBS), permeabilized, and blocked with 2% bovine serum albumin (BSA) plus 0.2% Triton X-100 in PBS for 1 h at 37°C. Immunofluorescence assay (IFA) was performed using murine polyclonal anti-Py-MIF and Alexa Fluor 596-conjugated murine anti-circumsporozoite protein (CSP) antibodies. In other instances, fluorescence staining was achieved with Alexa Fluor-conjugated secondary antibodies specific to rabbit and mouse IgGs. Nuclei were stained with DAPI (4′,6-diamidino-2-phenylindole). The slides were then mounted with FluoroGuard antifade reagent. Fluorescence and differential interference contrast (DIC) images were acquired using an Olympus 1×70 Delta Vision microscope equipped with deconvolution software.

(ii) *In vitro* IFA with HepG2-CD81 cells. Human hepatoma HepG2 cells expressing the tetraspanin CD81 (HepG2-CD81 cells) were plated on an 8-well chamber slide (Laboratory-Tek Permanox eight-well chamber slide; Nalge Nunc International, Rochester, NY) at a density of 5×10^4 cells/well overnight in DMEM with 10% fetal bovine serum (FBS) at 37°C and 5% CO_2. On the second day, salivary gland sporozoites dissected from mosquitoes infected with *P. yoelii* parasites were incubated with 20% FBS in RPMI 1640 medium for 30 min at room temperature. Next, 3×10^4 sporozoites were added to each well of the 8-well chamber slide cultured with HepG2-CD81 cells, with a subsequent spin at 2,000 rpm for 5 min at room temperature. Cells were incubated at 37°C and 5% CO_2 for 24 or 48 h, washed with PBS, and fixed with formalin. Cells were permeabilized and blocked with 2% BSA plus 0.2% Triton X-100 in PBS for 1 h at 37°C. IFA was performed using a rabbit polyclonal antibody (upregulated in infectious sporozoites gene 4 [UIS4] or anti-Py-falstatin antibody) and the anti-Py-MIF antibody. Fluorescence staining was achieved with Alexa Fluor-conjugated secondary antibodies specific to rabbit and mouse IgGs. Nuclei were stained with DAPI. The slides were then mounted with FluoroGuard antifade reagent. Fluorescence and DIC images were acquired using an Olympus 1×70 Delta Vision microscope equipped with deconvolution software.

(iii) Liver sections. To visualize *in vivo* development of *P. yoelii* WT or Δ*mif* parasites in livers, 6- to 8-week-old female BALB/cJ mice were injected intravenously with 1×10^6 WT or Δ*mif* sporozoites. Livers from the infected mice were harvested, washed extensively with PBS, and fixed in 4% paraformaldehyde (PFA) at several time points postinfection (p.i.) (2 h, 16 h, 30 h, 44 h, and 50 h). Fifty-micrometer sections were cut from fixed livers by use of a Vibratome apparatus (Ted Pella Inc., Redding, CA). IFAs were performed as previously described (46). Primary antibodies used in IFAs were rabbit polyclonal anti-falstatin or anti-UIS4 antibodies

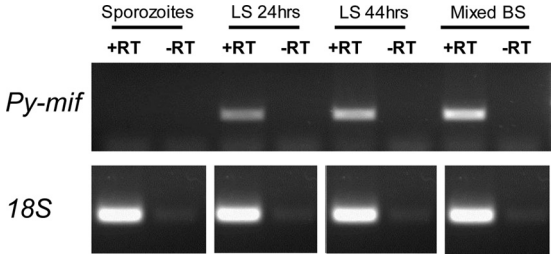

FIG 1 Py-MIF transcript is expressed in liver-stage (LS) and blood-stage (BS) parasites. The expression of Py-*mif* was determined by RT-PCR on RNA derived from *P. yoelii* 17XNL. RNA was isolated from salivary gland sporozoites, mixed blood-stage parasites, or mouse livers infected with 1×10^6 sporozoites (isolated at 24 or 44 hpi). Genomic DNA was removed by DNase treatment, and cDNA was generated by reverse transcriptase single-strand DNA synthesis. Either Py-*mif* or 18S rRNA was amplified from cDNAs via 35 cycles of PCR. Non-RT controls (−RT) were included to confirm that *mif* amplification was due to cDNA and not to residual genomic DNA.

paired with mouse anti-Py-MIF. Fluorescence staining was achieved with Alexa Fluor-conjugated secondary antibodies specific to rabbit and mouse IgGs. Nuclei were stained with DAPI. The slides were then mounted with FluoroGuard antifade reagent. Fluorescence and DIC images were acquired using an Olympus 1×70 Delta Vision microscope.

Blood-stage parasite growth curve. Blood from SW mice infected with *P. yoelii* WT or Δ*mif* parasites was harvested, diluted with RPMI 1640, and used to infect naïve SW mice for blood-stage growth analysis. One hundred microliters of diluted blood containing 1×10^6 parasites (WT or Δ*mif*) was injected intravenously into each experimental SW mouse (five mice in each group). Parasitemia was tracked by analyzing Giemsa-stained blood smears daily until clearance.

Statistics. Statistical analyses were performed on two or more independent experiments (unpaired two-tailed Student's *t* test), as noted in the figure legends or text. Significance indications are as follows: *, $0.01 < P < 0.05$; **, $0.001 < P < 0.01$; and ***, $P < 0.001$.

RESULTS

Py-MIF is expressed during liver stages. While several groups have determined that *Plasmodium* MIF is expressed in erythrocyte-stage parasites (2, 45), the expression pattern of MIF during pre-erythrocyte-stage infection had yet to be determined. To establish the expression pattern of Py-*mif* transcripts *in vivo*, we monitored Py-*mif* mRNA in the parasite life cycle by RT-PCR. Sporozoites were isolated from the salivary glands of infected *Anopheles stephensi* mosquitoes for RNA isolation or were injected into BALB/cJ mice intravenously via the tail vein. Blood or livers from the infected mice were removed after various time points for the isolation of RNA. Py-*mif* transcripts were detected in mixed blood-stage parasites and 24-h and 44-h liver-stage schizonts but were not observed in infectious salivary gland sporozoites after 35 amplification cycles (Fig. 1) or 45 cycles (see Fig. S1 in the supplemental material). Amplification of parasite 18S rRNA was used as a positive control (Fig. 1; see Fig. S1). We then established the protein expression dynamics and localization of Py-MIF in pre-erythrocyte-stage parasites *in vitro* by IFA using a polyclonal antibody raised against Py-MIF (45). Py-MIF was detected at low levels in salivary gland sporozoites, but its expression was strong in liver-stage schizonts (Fig. 2A to C). The small amounts of MIF observed in sporozoites (Fig. 2A) were not likely to be unspecific staining, since a similar pattern was observed in parasites expressing a myc-tagged version of Py-MIF by use of an anti-myc antibody (see Fig. S2). At 24 h postinfection (hpi), Py-MIF was distributed uniformly throughout the parasite cytoplasm (Fig. 2B). At 48 hpi, at which point nuclear centers had formed in the late schizonts, Py-MIF appeared to be restricted to the interior of the

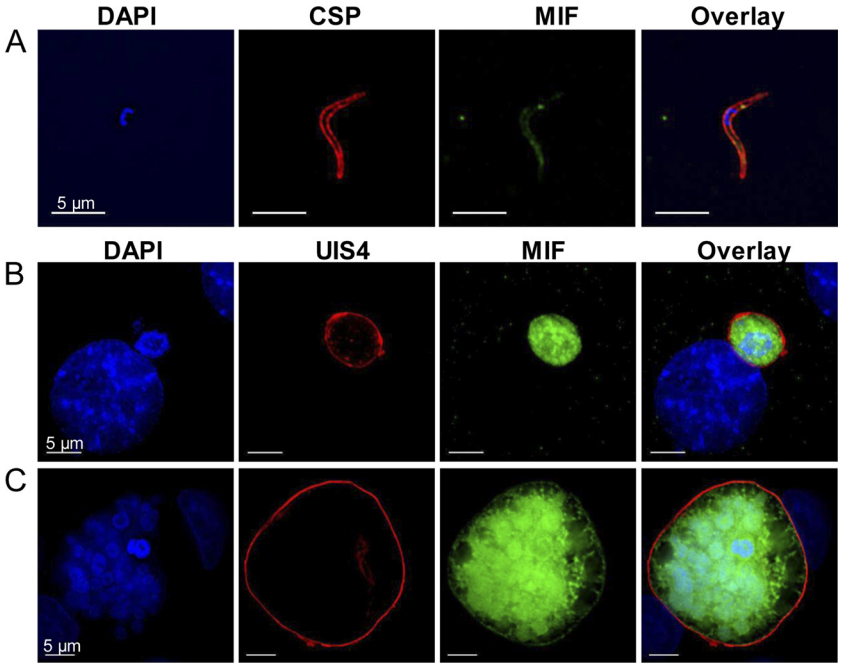

FIG 2 Localization of Py-MIF during *in vitro* liver-stage development. (A) *P. yoelii* sporozoites were isolated from salivary glands of *Anopheles stephensi* mosquitoes and stained with polyclonal mouse antibody to Py-MIF (green) and CSP (red). (B and C) HepG2-CD81 cells were infected with *P. yoelii* salivary gland sporozoites and fixed at 24 (B) or 48 (C) hpi. Cells were stained with a mouse anti-Py-MIF antibody (green), and a polyclonal rabbit anti-UIS4 antibody (red) was used to localize the parasitophorous vacuole membrane. DAPI (blue) was used to stain the nuclei of both parasites and host hepatocytes.

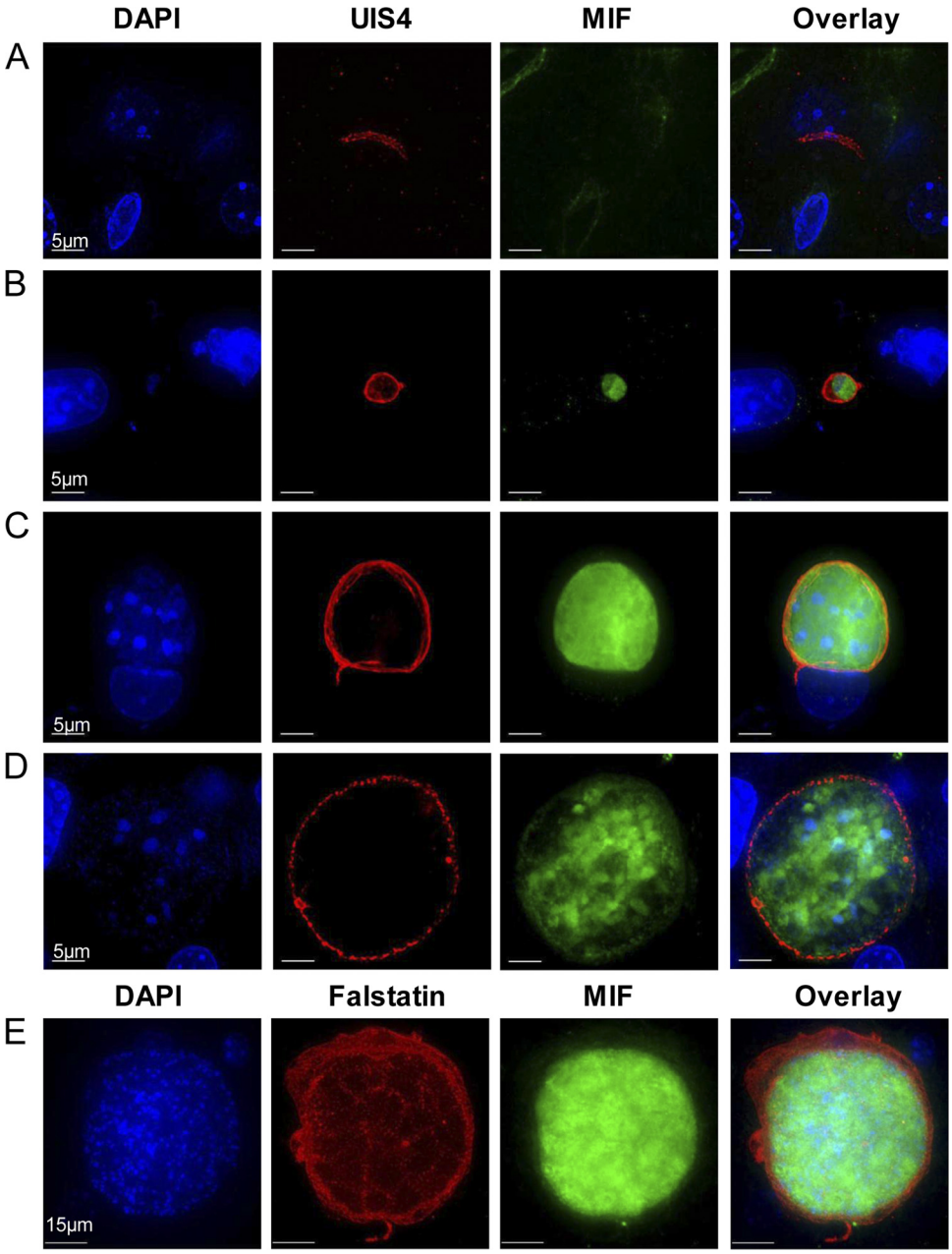

FIG 3 Localization of Py-MIF in liver-stage parasite mouse infections. One million *P. yoelii* Δ*mif* sporozoites were injected intravenously into BALB/cJ mice to study liver-stage development *in vivo*. Liver sections were stained at 2 (A), 16 (B), 30 (C), 44 (D), and 52 (E) hpi with a polyclonal mouse anti-Py-MIF antibody (green). (A to D) A polyclonal rabbit anti-UIS4 antibody (red) was used to localize the parasitophorous vacuole membrane of liver-stage parasites. (E) Cells were stained with a polyclonal rabbit antibody against Py-falstatin (red), a protein that is released into the host cell during late liver-stage development. DAPI was used to stain the nuclei of both parasites and host hepatocytes.

parasites and was concentrated in globular patterns (Fig. 2C). To confirm this pattern of expression *in vivo*, BALB/cJ mice were infected with 1×10^6 *P. yoelii* sporozoites, and their livers were harvested at increasing intervals postinfection. Py-MIF expression was monitored by IFA. We were unable to detect Py-MIF expression at an early time point *in vivo* (2 hpi) (Fig. 3A); however, Py-MIF was clearly present at later developmental stages (Fig. 3B to E). In 16-h and 30-h liver-stage schizonts, MIF exhibited a uniform distribution throughout the parasite (Fig. 3B and C), while at a later time point (44 hpi) Py-MIF became more compartmentalized and the distribution was focused in the nuclear centers (Fig. 3D). Throughout the exoerythrocytic stages, Py-MIF staining was always observed within the confines of the parasite and never within the host cell, as shown by staining with antibodies against the parasitophorous vacuole membrane (PVM) marker UIS4 (32) (Fig. 2 and 3). However, the parasite plasma membrane is in close proximity to the PVM. Thus, it was difficult to determine whether some MIF was also found in the vacuolar lumen. During blood-stage development, Py-MIF is released or secreted from the parasite during schizont rupture (45). To determine if

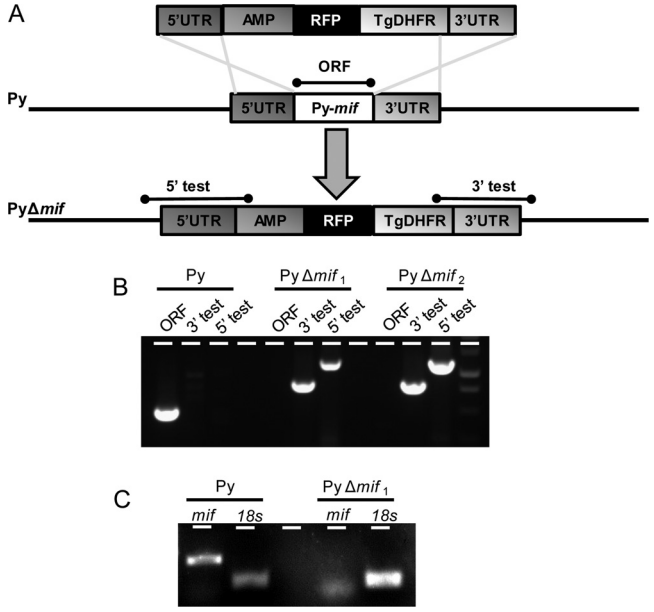

FIG 4 Generation of *P. yoelii* Δ*mif* parasites. (A) Py-*mif* was replaced with a selectable drug resistance marker (TgDHFR, the *dhfr* gene from *Toxoplasma gondii* [positive selection marker]; and AMP, ampicillin resistance gene for bacterial selection) and a cassette encoding red fluorescent protein by double-crossover homologous recombination using the 5′UTR and 3′UTR regions at the Py-*mif* locus. The resulting *mif*-deficient parasite population was fluorescent red. (B) The mixed population of wild-type and transgenic parasites was cloned by serial limiting dilution into SW mice. The genotyping gel shows successful integration on the 3′ (3′ test) and 5′ (5′ test) flanks, as well as the loss of the Py-*mif* open reading frame, in two independent clones (PyΔmif_1 and PyΔmif_2). (C) RT-PCR using primers amplifying either *mif* or 18S rRNA from WT or *P. yoelii* Δmif_1 blood-stage parasites. RT-PCR was performed on cDNA derived from 1 μg of parasite RNA.

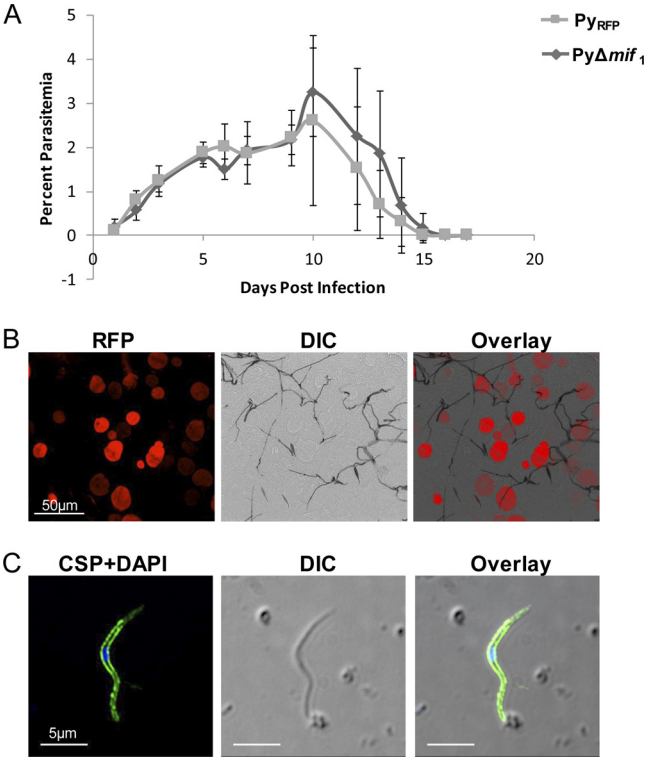

FIG 5 *mif*-deficient parasites develop normally during mosquito or blood stages. (A) Blood-stage growth curve. One million control or *P. yoelii* Δmif_1 blood-stage parasites were injected into BALB/c mice, and parasitemia in the blood was measured daily until all parasites were cleared. (B) *P. yoelii* Δ*mif* parasites form oocysts. Midguts from mosquitoes infected with the *P. yoelii* Δmif_1 strain were collected at 10 days p.i. and viewed by fluorescence microscopy. *P. yoelii* Δ*mif* oocysts are fluorescent red. (C) *P. yoelii* Δ*mif* strain generates salivary gland sporozoites. *P. yoelii* Δmif_1 sporozoites were isolated from mosquito salivary glands and stained with a mouse polyclonal antibody against CSP (green). Parasite DNA was stained with DAPI (blue).

Py-MIF is released during late liver-stage development, we compared the distribution of Py-MIF to that of Py-falstatin, a protein that is secreted into the PV and released into the host cell during late liver-stage development (35; Y. Pei et al., unpublished data). At 50 hpi, when Py-falstatin was released into the host cell, Py-MIF was still contained within the parasite (Fig. 3E), suggesting that Py-MIF is likely confined to the parasite cytoplasm and not exported beyond the parasite plasma membrane.

Generation of *P. yoelii* Δ*mif* parasites. To determine if Py-MIF is important for liver-stage development, we generated a Py-*mif* knockout in *P. yoelii* (*P. yoelii* Δ*mif*). Using a double-crossover recombination strategy, the *mif* locus was replaced with a selectable marker (dihydrofolate reductase [DHFR]) and an RFP cassette under the control of a constitutive promoter (30) (Fig. 4A). The recombinant parasites were cloned by serial dilution, and the clonal identity of two parasite lines (*P. yoelii* Δmif_1 and *P. yoelii* Δmif_2 clones), derived from two independent transfections, was confirmed by PCR (Fig. 4B). To verify that Py-*mif* expression was completely ablated from *P. yoelii* Δ*mif* parasites, we also monitored Py-*mif* mRNA expression by RT-PCR. We were unable to detect Py-*mif* transcripts in the knockout clones (Fig. 4C). The gene knockout was also confirmed by the inability to detect Py-MIF by either IFA or Western blotting using a polyclonal Py-MIF antibody (see Fig. S3 in the supplemental material).

***P. yoelii* Δ*mif* strain is not attenuated during intraerythrocytic growth and shows normal development of mosquito-stage parasites.** In order to determine if deletion of Py-*mif* affected the blood-stage development of *P. yoelii*, we monitored the parasitemia of BALB/cJ mice infected with *P. yoelii* Δ*mif* parasites. The growth curve was compared to that of an RFP-expressing control parasite in which an RFP expression cassette was inserted into the dispensable S1 locus (19). These parasites were comparable to WT parasites (19) and heretofore are designated control parasites. Mice were injected with 1×10^6 blood-stage parasites, and the resulting parasitemia was determined daily by counting Giemsa-stained parasites in a thin blood smear. No differences were observed between the growth rates of *P. yoelii* Δ*mif* parasites and the RFP-expressing control parasites (Fig. 5A). Peak parasitemia of mice infected with control parasites was slightly higher than that of mice infected with the knockout strain; however, this difference was not statistically significant (*P. yoelii* Δ*mif* parasitemia = 2.60% ± 1.93%; control parasitemia = 3.25% ± 1.01%; $P = 0.73$). Next, we determined if the *P. yoelii* Δ*mif* strain was defective during mosquito-stage development. *Anopheles stephensi* mosquitoes were fed on SW mice infected with two independent clones of the *P. yoelii* Δ*mif* strain or control *P. yoelii* parasites. Mosquito midguts and salivary glands were harvested and analyzed after 10 and 14 days, respectively. *P. yoelii* Δ*mif* parasites formed oocysts (Fig. 5B) and generated oocyst sporozoites similarly to WT *P.*

TABLE 1 Deletion of Py-*mif* does not affect sporozoite development in *Anopheles* mosquitoes

Genotype	No. of sporozoites per mosquito[a]	
	Oocysts[b]	Salivary glands[c]
RFP-expressing WT	65,800 ± 26,543	17,275 ± 7,864
Δ*mif*$_1$	81,500 ± 37,772	20,383 ± 9,442
Δ*mif*$_2$	64,083 ± 18,304	15,016 ± 7,311

[a] Values are means ± standard deviations.
[b] Mosquito midguts were removed at 10 days p.i., and oocyst sporozoites were quantified (combination of 3 independent experiments, with >30 mosquitoes per experiment).
[c] Salivary gland sporozoites were dissected at 14 days p.i. and quantified (combination of 4 independent experiments, with >30 mosquitoes per experiment).

yoelii (Table 1). There were also no significant differences in the number or appearance of salivary gland sporozoites produced in *P. yoelii* Δ*mif* strain- or WT-infected mosquitoes (Fig. 5C; Table 1).

***P. yoelii* Δ*mif* parasites show a liver-stage growth defect.** Since Py-MIF is highly expressed in liver-stage parasites, we hypothesized that it might have an important function in this stage. First, we determined if *P. yoelii* Δ*mif* parasites were able to complete liver-stage development. BALB/cJ mice were injected intravenously with 1×10^3 or 1×10^4 sporozoites of either control *P. yoelii* or *P. yoelii* Δ*mif*$_1$ and *P. yoelii* Δ*mif*$_2$, and the onset of blood-stage parasitemia was monitored by evaluating thin blood smears. All of the mice infected with the control parasites developed blood-stage patency at approximately 3 days post-sporozoite injection (Table 2). However, less than 50% of mice infected with 1×10^3 *P. yoelii* Δ*mif* sporozoites had become patent up to the conclusion of the experiment at 20 days postinfection. For mice that became patent, the onset of blood-stage parasitemia was delayed 2 days compared to that with the control, signifying a dramatic reduction in the number of infectious exoerythrocytic merozoites produced by the *P. yoelii* Δ*mif* strain. Patency was more frequent in mice after injecting 1×10^4 *P. yoelii* Δ*mif* sporozoites, and the onset of patency was delayed 1 day in mice that did develop blood-stage infection (Table 2).

To determine the nature of the liver-stage defect in the *P. yoelii* Δ*mif* strain, we first quantified the biomass of *P. yoelii* Δ*mif* parasites in the liver compared to that for control *P. yoelii* by QPCR. RNA was isolated from the livers of BALB/cJ mice infected with 1×10^6 *P. yoelii* Δ*mif* or control sporozoites at 44 hpi. The parasite mass was quantified by monitoring the abundance of parasite 18S rRNA compared to total liver RNA (measured by using mouse *GAPDH*). The *P. yoelii* Δ*mif* data were further normalized to the abundance levels of the control parasite, which were set to 1. Livers of mice infected with the *P. yoelii* Δ*mif* strain contained significantly less parasite RNA than those infected with the control parasite (for *P. yoelii*, 1 ± 0.20 normalized units; for *P. yoelii* Δ*mif* strain, 0.42 ± 0.28 normalized units), confirming a growth defect of *P. yoelii* Δ*mif* parasites (Fig. 6). To evaluate if the reduced liver-stage burden observed for *P. yoelii* Δ*mif* parasites was due to a defect in initial infection of the liver, the parasite-infected livers were examined by IFA on liver sections. Fewer *P. yoelii* Δ*mif* liver-stage parasites than control parasites were observed in mouse livers; however, these differences were not statistically significant (Fig. 7A). Thus, the initial steps of hepatocyte invasion and dedifferentiation into a trophozoite appeared not to be affected significantly by the deletion of *mif*. However, further microscopic evaluation of infected livers revealed that the *P. yoelii* Δ*mif* parasites were significantly smaller than control *P. yoelii* parasites at 44 hpi (Fig. 7B and C), with the average diameter of a control parasite being 40.1 ± 10.3 μm and the diameter of a *mif*-deficient parasite being 24.9 ± 7.6 μm (Fig. 7C). We also attempted to evaluate the final phases of liver-stage development, such as merosome formation or merozoite release, in the *P. yoelii* Δ*mif* parasites. We were unable to detect the presence of merosomes in either *P. yoelii* Δ*mif* or WT parasites in liver sections (data not shown). However, this absence of merosomes was likely due to the technical difficulty of observing merosome formation in *P. yoelii in vivo* and not indicative of the ability of *P. yoelii* Δ*mif* parasites to produce them. It is important to restate here that functional merozoites can be produced by *P. yoelii* Δ*mif* liver-stage parasites, as some mice infected with the *P. yoelii* Δ*mif* sporozoites developed blood-stage patency (Table 2).

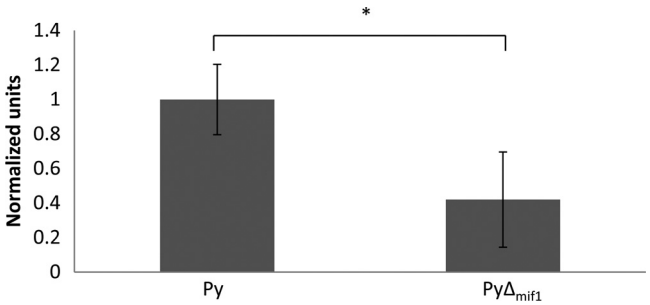

FIG 6 Livers from mice infected with the *P. yoelii* Δ*mif* strain contain less parasite biomass than those infected with WT *P. yoelii*. BALB/cJ mice were infected with 1×10^6 WT (Py) or *mif*-deficient clone 1 (PyΔ*mif*$_1$) *P. yoelii* sporozoites. Livers were harvested at 44 hpi, and the relative amounts of parasite biomass were determined by QPCR for 18S rRNA and normalized to the wild type. Data for a representative sample of two repetitions are shown (n = 5 mice per group). *, $P < 0.05$.

TABLE 2 Delayed patency in BALB/c mice infected with *P. yoelii* Δ*mif* parasites compared to those infected with control parasites

Genotype	Dose[a]	No. of mice injected	% Patent mice[b]	Mean days to patency[b]
RFP-expressing WT	10^4	14	100	3.0
	10^3	14	100	3.5
Δ*mif*$_1$	10^4	12	83	4.4
	10^3	12	50	5.4
Δ*mif*$_2$	10^4	15	47	3.8
	10^3	15	40	5.5

[a] Number of sporozoites injected per mouse.
[b] Blood-stage patency was monitored in mice by daily thin smears.

DISCUSSION

MIF is a pleiotropic factor that plays important roles in mammalian immune responses (8). *Plasmodium* parasites express a MIF homologue; however, the importance of this protein during infection has yet to be delineated clearly (2, 11, 40, 45). Here we characterized a MIF homologue from *P. yoelii* throughout the parasite life cycle and determined a role for it during liver-stage malaria infection.

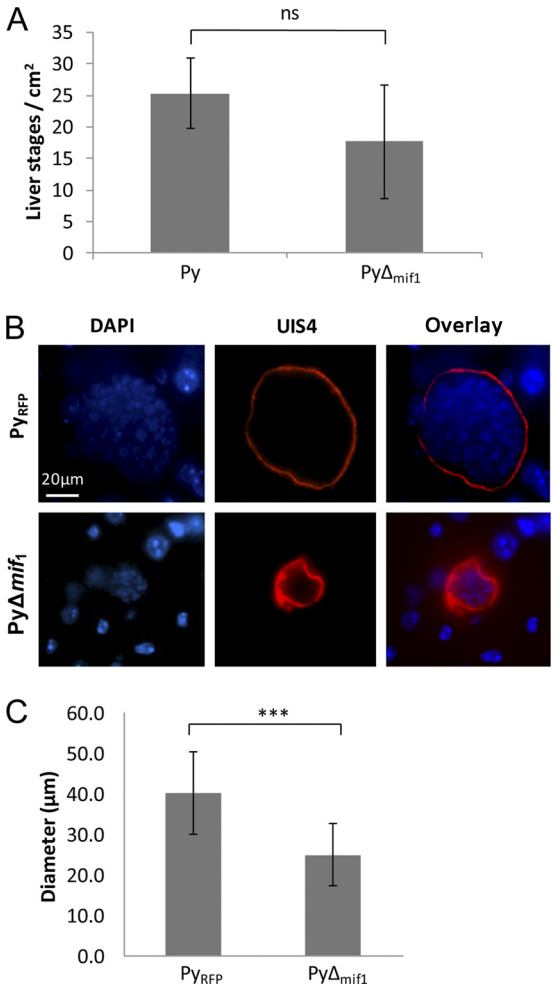

FIG 7 Py-*mif*-deficient liver-stage parasites exhibit a growth defect. (A and B) Livers from mice infected with 1×10^6 *P. yoelii* WT or Δ*mif* parasites were analyzed at 44 hpi. (A) Quantification of the number of liver-stage parasites per cm^2 of liver (for WT, 25 ± 5.60; for *P. yoelii* Δ*mif* strain, 17.67 ± 8.31; $P = 0.09$). The data are combinations for 2 experimental replicates. ns, not significant. (B) Liver sections were stained with a rabbit polyclonal antibody against UIS4 (red) to mark the parasitophorous vacuole membrane in infected hepatocytes. DNA is stained with DAPI (blue). Images of a representative sample are shown. (C) Diameters of RFP-expressing *P. yoelii* control ($n = 18$) and *P. yoelii* Δ*mif* ($n = 21$) parasites were measured using the ruler tool in the Metamorph software package. Three or four diameters were measured for each parasite and then averaged. ***, $P < 0.001$.

During blood-stage replication, *Plasmodium* MIF is expressed in trophozoites and schizonts and is released during schizont rupture (2, 16, 39). It has been reported that Pf-MIF localizes to Mauer's clefts and is detectable in the cytoplasm of the host erythrocyte (11); however, this localization was not observed with Py-MIF, which was detected only in the parasite cytoplasm (45). *P. berghei* MIF expression has also been observed in mosquito midgut oocysts and in salivary gland sporozoites (2). Here we show for the first time the expression of *Plasmodium* MIF in liver-stage parasites. Py-MIF protein was expressed weakly in sporozoites assayed by IFA, but *mif* transcripts were not detected in salivary gland sporozoites by RT-PCR, as they may have been present in amounts below the limit of detection. Furthermore, we did not detect Py-MIF at 2 h post-hepatocyte invasion *in vivo*. However, during liver-stage development, Py-MIF was expressed in increasing amounts and was localized within the parasite. During late liver-stage development, Py-MIF exhibited a globular staining pattern within the parasite and was associated with the numerous nuclear DNA masses. At no point did we detect Py-MIF in the host hepatocyte cytoplasm, even during late stages, when secreted proteins such as Py-falstatin are released (Pei et al., unpublished data). To further characterize Py-MIF in liver-stage parasites, we generated a Py-*mif* knockout strain which showed no difference in blood-stage growth rate or in the generation of mosquito oocyst or salivary gland sporozoites compared to a control parasite line with normal development. However, *mif*-deficient parasites were defective in liver-stage growth, as shown by the delay or lack of patency observed in mice injected with *P. yoelii* Δ*mif* sporozoites. Also, *mif*-deficient parasites were significantly smaller than control parasites at late time points of liver-stage development, suggesting that *P. yoelii* Δ*mif* parasites do not suffer a defect during initial infection but during subsequent liver-stage growth. In contrast, Augustijn et al. created a *mif* knockout in *P. berghei* and stated that it was comparable to the WT throughout the parasite life cycle. However, no data were shown for liver-stage infection (2). It is possible that a liver-stage phenotype may not have been obvious if large numbers of sporozoites were injected into mice; however, it is difficult to speculate due to insufficient data published for the *P. berghei* system.

Several groups have shown that *Plasmodium* MIF can modulate host cells by inducing chemotaxis of macrophages or cell signaling or inhibiting apoptosis (2, 11, 40, 45). However, all of these findings are based on experiments with recombinant MIF. We found that Py-MIF is confined within the parasite in *P. yoelii* liver-stage parasites throughout development *in vivo*. We did not observe secretion of Py-MIF at any point during liver-stage development, including the late stages, when the PVM breaks down and allows access of proteins in the vacuolar lumen to the host cell cytoplasm. Thus, Py-MIF would not have access to external host receptors or other cell types in the liver on which it could exert cytokine- or chemokine-like functions. This suggests that Py-MIF has parasite-endogenous functions and likely does not interact with external host factors during the liver stage. While it is established that *Plasmodium* MIF has the intrinsic ability to modulate host cell responses, there is no direct evidence to suggest that MIF interacts physically with host factors *in vivo*. We cannot rule out the possibility that MIF interacts with host factors during the parasite erythrocytic cycle, as some groups have suggested that *Plasmodium* MIF is secreted during blood stages (2, 39, 45). However, direct evidence of any such interactions *in vivo* has yet to be demonstrated.

Mammalian MIF has multiple functions, ranging from cytokine and chemokine properties to regulation of the cell cycle (reviewed in references 10 and 33). It is unlikely that Py-MIF modulates host immune responses through its cytokine or chemokine functions during liver stages because of its intracellular localization in the parasite. However, it is possible that Py-MIF may play a role in parasite survival through its intracellular functions, such as its ability to regulate cell division. In mammalian cells, MIF modulates the cell cycle through its interaction with JAB-1, a protein involved in the proteasomal regulation of cyclins necessary for cell cycle progression. The MIF–Jab-1 interaction is particularly important in the coordination of cell cycle checkpoints, and in MIF-deficient cells, the proteasome is uncoupled from check-

points in the event of DNA damage (reviewed in reference 33). Thus, MIF-deficient *Plasmodium* parasites may be unable to efficiently regulate cell division after sustaining DNA damage generated during the normal course of cellular metabolism and may continue through the cell cycle despite DNA damage. This would result in the accumulation of DNA mutations, which may lead to unhealthy or developmentally delayed parasites. The smaller parasites observed in the livers of *P. yoelii* Δ*mif* parasite-infected mice may have been due to such an accumulation of DNA damage. It would be interesting to determine if *P. yoelii* Δ*mif* parasites have a higher mutation rate than WT parasites.

In addition to its possible function in regulating the cell cycle, MIF may also be involved in protection from host cell-generated reactive oxygen species (ROS). Cells generate ROS in response to pathogens via the NADPH oxidase (12, 15). These ROS can be delivered directly into pathogen-containing vesicles, and several species, such as H_2O_2 and nitric oxide, can pass freely through cell membranes. Also, inducible nitric oxide synthase has been observed in *P. berghei*-infected hepatocytes and may deliver microbicidal nitric oxide directly into the PV (25). MIF possesses a thioredoxin-like oxidoreductase active site. In mammals, thioredoxin-like activity is thought to be important for cellular redox homeostasis, ROS neutralization, and apoptosis inhibition (reviewed in reference 44). Crystal structures for Pb-MIF and Pf-MIF show that the second cysteine (Cys59) of the catalytic CALC motif, thought to be necessary for oxidoreductase activity in mammalian MIF, is not accessible in the parasite homologs (13). However, recent evidence suggests that Pf-MIF may retain oxidoreductase activity through two N-terminal cysteines (Cys3 and Cys4) (1). Thus, another possible role for Py-MIF in liver-stage parasites may be through the antioxidant functions of its oxidoreductase site. Pf-MIF possesses antioxidant functions, as it prevented reactive oxygen species-mediated lipid peroxidation and oxidative damage of DNA *in vitro* (1). In the absence of MIF, reactive oxygen species or other oxidizing agents may build up in the parasite, inducing DNA damage and/or growth arrest.

Further research remains to determine the specific functions and mechanisms of action of parasite MIF. The importance of MIF in liver-stage parasites determined by our work will help to refocus future experiments to elucidate the role of MIF in the parasite life cycle.

ACKNOWLEDGMENTS

This work was supported by internal funding from Seattle BioMed.

We thank Jim Burns for providing us with the *P. yoelii* MIF polyclonal antisera.

REFERENCES

1. **Alam A, et al.** 2011. Cysteine-3 and cysteine-4 are essential for the thioredoxin-like oxidoreductase and antioxidant activities of Plasmodium falciparum macrophage migration inhibitory factor. Free Radic. Biol. Med. **50**:1659–1668.
2. **Augustijn KD, et al.** 2007. Functional characterization of the Plasmodium falciparum and P. berghei homologues of macrophage migration inhibitory factor. Infect. Immun. **75**:1116–1128.
3. **Awandare GA, et al.** 2006. A macrophage migration inhibitory factor promoter polymorphism is associated with high-density parasitemia in children with malaria. Genes Immun. **7**:568–575.
4. **Bacher M, et al.** 1996. An essential regulatory role for macrophage migration inhibitory factor in T-cell activation. Proc. Natl. Acad. Sci. U. S. A. **93**:7849–7854.
5. **Bernhagen J, Calandra T, Cerami A, Bucala R.** 1994. Macrophage migration inhibitory factor is a neuroendocrine mediator of endotoxaemia. Trends Microbiol. **2**:198–201.
6. **Bernhagen J, et al.** 2007. MIF is a noncognate ligand of CXC chemokine receptors in inflammatory and atherogenic cell recruitment. Nat. Med. **13**:587–596.
7. **Bozza M, et al.** 1999. Targeted disruption of migration inhibitory factor gene reveals its critical role in sepsis. J. Exp. Med. **189**:341–346.
8. **Calandra T.** 2003. Macrophage migration inhibitory factor and host innate immune responses to microbes. Scand. J. Infect. Dis. **35**:573–576.
9. **Calandra T, Bernhagen J, Mitchell RA, Bucala R.** 1994. The macrophage is an important and previously unrecognized source of macrophage migration inhibitory factor. J. Exp. Med. **179**:1895–1902.
10. **Conroy H, Mawhinney L, Donnelly SC.** 2010. Inflammation and cancer: macrophage migration inhibitory factor (MIF)—the potential missing link. QJM **103**:831–836.
11. **Cordery DV, et al.** 2007. Characterization of a Plasmodium falciparum macrophage-migration inhibitory factor homologue. J. Infect. Dis. **195**: 905–912.
12. **de Mochel NS, et al.** 2010. Hepatocyte NAD(P)H oxidases as an endogenous source of reactive oxygen species during hepatitis C virus infection. Hepatology **52**:47–59.
13. **Dobson SE, et al.** 2009. The crystal structures of macrophage migration inhibitory factor from Plasmodium falciparum and Plasmodium berghei. Protein Sci. **18**:2578–2591.
14. **Fingerle-Rowson G, et al.** 2009. A tautomerase-null macrophage migration-inhibitory factor (MIF) gene knock-in mouse model reveals that protein interactions and not enzymatic activity mediate MIF-dependent growth regulation. Mol. Cell. Biol. **29**:1922–1932.
15. **Grandvaux N, Soucy-Faulkner A, Fink K.** 2007. Innate host defense: Nox and Duox on phox's tail. Biochimie **89**:1113–1122.
16. **Han C, et al.** 2010. Plasma concentration of malaria parasite-derived macrophage migration inhibitory factor in uncomplicated malaria patients correlates with parasitemia and disease severity. Clin. Vaccine Immunol. **17**:1524–1532.
17. **Hudson JD, et al.** 1999. A proinflammatory cytokine inhibits p53 tumor suppressor activity. J. Exp. Med. **190**:1375–1382.
18. **Imamura K, et al.** 1996. Identification and immunohistochemical localization of macrophage migration inhibitory factor in human kidney. Biochem. Mol. Biol. Int. **40**:1233–1242.
19. **Jacobs-Lorena VY, Mikolajczak SA, Labaied M, Vaughan AM, Kappe SH.** 2010. A dispensable Plasmodium locus for stable transgene expression. Mol. Biochem. Parasitol. **171**:40–44.
20. **Janse CJ, et al.** 2006. High efficiency transfection of Plasmodium berghei facilitates novel selection procedures. Mol. Biochem. Parasitol. **145**:60–70.
21. **Kamir D, et al.** 2008. A Leishmania ortholog of macrophage migration inhibitory factor modulates host macrophage responses. J. Immunol. **180**: 8250–8261.
22. **Kanai T, et al.** 2003. Macrophage-derived IL-18 targeting for the treatment of Crohn's disease. Curr. Drug Targets Inflamm. Allergy **2**:131–136.
23. **Kleemann R, et al.** 2000. Intracellular action of the cytokine MIF to modulate AP-1 activity and the cell cycle through Jab1. Nature **408**:211–216.
24. **Kleemann R, et al.** 1998. Disulfide analysis reveals a role for macrophage migration inhibitory factor (MIF) as thiol-protein oxidoreductase. J. Mol. Biol. **280**:85–102.
25. **Klotz FW, et al.** 1995. Co-localization of inducible-nitric oxide synthase and Plasmodium berghei in hepatocytes from rats immunized with irradiated sporozoites. J. Immunol. **154**:3391–3395.
26. **Labaied M, Camargo N, Kappe SH.** 2007. Depletion of the Plasmodium berghei thrombospondin-related sporozoite protein reveals a role in host cell entry by sporozoites. Mol. Biochem. Parasitol. **153**:158–166.
27. **Leng L, et al.** 2003. MIF signal transduction initiated by binding to CD74. J. Exp. Med. **197**:1467–1476.
28. **Lue H, Kleemann R, Calandra T, Roger T, Bernhagen J.** 2002. Macrophage migration inhibitory factor (MIF): mechanisms of action and role in disease. Microbes Infect. **4**:449–460.
29. **McDevitt MA, et al.** 2006. A critical role for the host mediator macrophage migration inhibitory factor in the pathogenesis of malarial anemia. J. Exp. Med. **203**:1185–1196.
30. **Mikolajczak SA, Aly AS, Dumpit RF, Vaughan AM, Kappe SH.** 2008. An efficient strategy for gene targeting and phenotypic assessment in the Plas-

modium yoelii rodent malaria model. Mol. Biochem. Parasitol. **158**:213–216.
31. **Mikolajczak SA, Kappe SH.** 2006. A clash to conquer: the malaria parasite liver infection. Mol. Microbiol. **62**:1499–1506.
32. **Mueller AK, et al.** 2005. Plasmodium liver stage developmental arrest by depletion of a protein at the parasite-host interface. Proc. Natl. Acad. Sci. U. S. A. **102**:3022–3027.
33. **Nemajerova A, Moll UM, Petrenko O, Fingerle-Rowson G.** 2007. Macrophage migration inhibitory factor coordinates DNA damage response with the proteasomal control of the cell cycle. Cell Cycle **6**:1030–1034.
34. **Noels H, Bernhagen J, Weber C.** 2009. Macrophage migration inhibitory factor: a noncanonical chemokine important in atherosclerosis. Trends Cardiovasc. Med. **19**:76–86.
35. **Rennenberg A, et al.** 2010. Exoerythrocytic Plasmodium parasites secrete a cysteine protease inhibitor involved in sporozoite invasion and capable of blocking cell death of host hepatocytes. PLoS Pathog. **6**:e1000825.
36. **Rosengren E, et al.** 1996. The immunoregulatory mediator macrophage migration inhibitory factor (MIF) catalyzes a tautomerization reaction. Mol. Med. **2**:143–149.
37. **Salminen A, Kaarniranta K.** 2011. Control of p53 and NF-kappaB signaling by WIP1 and MIF: role in cellular senescence and organismal aging. Cell. Signal. **23**:747–752.
38. **Schober A, Bernhagen J, Weber C.** 2008. Chemokine-like functions of MIF in atherosclerosis. J. Mol. Med. (Berlin) **86**:761–770.
39. **Shao D, et al.** 2008. Detection of Plasmodium falciparum derived macrophage migration inhibitory factor homologue in the sera of malaria patients. Acta Trop. **106**:9–15.
40. **Shao D, et al.** 2010. Structural and functional comparison of MIF ortholog from Plasmodium yoelii with MIF from its rodent host. Mol. Immunol. **47**:726–737.
41. **Shi X, et al.** 2006. CD44 is the signaling component of the macrophage migration inhibitory factor-CD74 receptor complex. Immunity **25**:595–606.
42. **Silvie O, et al.** 2006. Expression of human CD81 differently affects host cell susceptibility to malaria sporozoites depending on the Plasmodium species. Cell. Microbiol. **8**:1134–1146.
43. **Tarun AS, et al.** 2007. Protracted sterile protection with Plasmodium yoelii pre-erythrocytic genetically attenuated parasite malaria vaccines is independent of significant liver-stage persistence and is mediated by CD8+ T cells. J. Infect. Dis. **196**:608–616.
44. **Thiele M, Bernhagen J.** 2005. Link between macrophage migration inhibitory factor and cellular redox regulation. Antioxid. Redox Signal. **7**:1234–1248.
45. **Thorat S, Daly TM, Bergman LW, Burns JM, Jr.** 2010. Elevated levels of the Plasmodium yoelii homologue of macrophage migration inhibitory factor attenuate blood-stage malaria. Infect. Immun. **78**:5151–5162.
46. **Vaughan AM, et al.** 2009. Type II fatty acid synthesis is essential only for malaria parasite late liver stage development. Cell. Microbiol. **11**:506–520.
47. **Vermeire JJ, Cho Y, Lolis E, Bucala R, Cappello M.** 2008. Orthologs of macrophage migration inhibitory factor from parasitic nematodes. Trends Parasitol. **24**:355–363.
48. **Weiss WR, Good MF, Hollingdale MR, Miller LH, Berzofsky JA.** 1989. Genetic control of immunity to Plasmodium yoelii sporozoites. J. Immunol. **143**:4263–4266.
49. **WHO.** 2010. World malaria report. World Health Organization, Geneva, Switzerland.